Lacunarity transition in a chaotic dynamical system

OPEN ACCESS
IOP Publishing
Journal of Physics A: Mathematical and Theoretical
J. Phys. A: Math. Theor. **55** (2022) 335001 (17pp)
https://doi.org/10.1088/1751-8121/ac7f6a

Lacunarity transition in a chaotic dynamical system

Bartomeu Cucurull[1], Marc Pradas[1] and Michael Wilkinson[1,2,*]

[1] School of Mathematics and Statistics, The Open University, Walton Hall, Milton Keynes MK7 6AA, United Kingdom
[2] Chan Zuckerberg Biohub, 499 Illinois Street, San Francisco, CA 94158, United States of America

E-mail: m.wilkinson@open.ac.uk

Received 25 February 2022, revised 16 June 2022
Accepted for publication 7 July 2022
Published 5 August 2022

Abstract

Experiments investigating particles floating on a randomly stirred fluid show regions of very low density, which are not well understood. We introduce a simplified model for understanding sparsely occupied regions of the phase space of non-autonomous, chaotic dynamical systems, based upon an extension of the skinny bakers' map. We show how the distribution of the sizes of voids in the phase space can be mapped to the statistics of the running maximum of a Wiener process. We find that the model exhibits a *lacunarity transition*, which is characterised by regions of the phase space remaining empty as the number of trajectories is increased.

Keywords: lacunarity, chaotic systems, diffusion process

(Some figures may appear in colour only in the online journal)

1. Introduction

Very small particles floating on a chaotically stirred liquid [1, 2] show regions where there is accumulation into regions of very high density, which are well described by fractal measures [1, 3]. These experiments also show regions of very low density, which were characterised in the paper by Larkin *et al* [2], but which are not yet well understood. Figure 1 illustrates the *lacunarity* of these chaotic attractors, by plotting 10^7 trajectories of a dynamical system

*Author to whom any correspondence should be addressed.

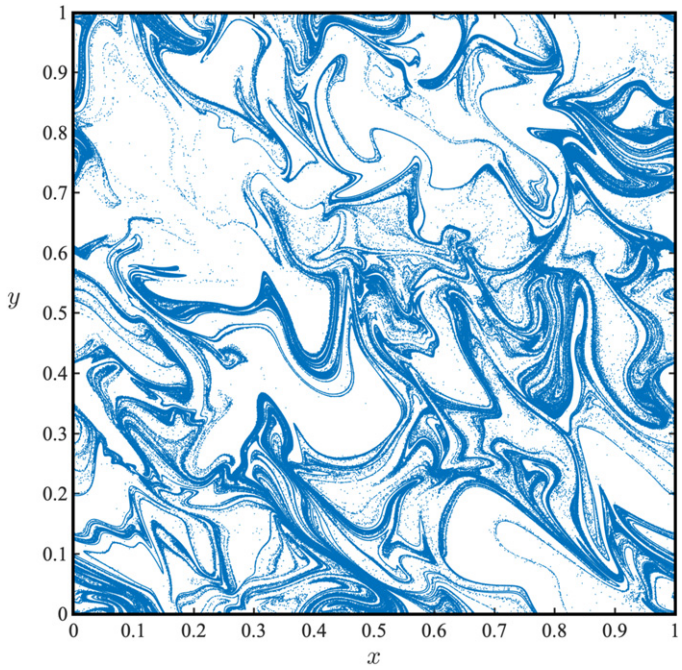

Figure 1. A model for particles floating on the surface of a randomly stirred fluid exhibits regions which are very sparsely occupied. This simulation represents the model discussed in [5] (with compressibility parameter $\beta = 0.5$ in the notation of that paper). We plot positions of $M = 10^7$ trajectories, at a representative large time, which were initially a uniform random scatter. Note that there are substantial voids, which contain no trajectories.

which mimics the motion of particles floating on the surface of a randomly stirred fluid (the equations defining the model are the same as those considered in [4, 5], see appendix A for further details). The concept of *lacunarity*, characterising the tendency of some complex sets to have sparsely populated regions, was introduced by Benoit Mandelbrot in his classic book on fractals [6], but its influence has not been as far-reaching as the fractal dimension. This is perhaps because there is not a single agreed definition of how lacunarity should be quantified: see [7, 8] for a discussion of some definitions of lacunarity.

The fractal dimension concept has been extended to 'multifractal' measures, which are considered to have different scaling exponent α in the vicinity of each point, and with the set of points with exponent α being a fractal with dimension $f(\alpha)$ [9, 10]. If this model is valid, the function $f(\alpha)$ is obtained by a Legendre transform of the Renyi dimension, as discussed in [9, 10]. The extent to which our results are consistent with this model is considered in our concluding remarks, section 6. A recent paper [11] considered sets arising as attractors of chaotic dynamical systems, and showed evidence that distribution of low densities has a power-law probability density function (PDF). The exponent of this power-law was termed the *lacunarity exponent*. However, the model considered in that work was fundamentally different because its dynamics was many-to-one (as a result of *folds* or *caustics*), whereas here we consider a dynamical system which is *invertible*. The theoretical arguments supporting the power-law described in [11] are critically dependent upon the non-invertible nature of the systems which were considered there.

This paper will introduce and analyse a simple model for invertible, non-autonomous, chaotic dynamical systems, such as the surface flow of a chaotically stirred fluid. The model is an extension of the skinny bakers' map, which is used as a minimal model for discussing fractality of chaotic attractors [3, 12]. Our model, which will be referred to as the *strudel model*, differs from the skinny bakers' map in two respects. Firstly, unlike the skinny bakers' map, it is invertible: there are no inaccessible regions of the phase space. Secondly, the discontinuities are introduced at random positions. Introducing this random element has two advantages. Firstly, it makes the phase space homogeneous, after averaging over the random parameters of the map. Secondly, the randomness facilitates our analysis of the system by enabling the use of statistical methods.

Here we describe sparse regions by considering the distribution of $M \gg 1$ trajectories, and considering the statistics of the size ϵ of the trajectory-free void surrounding an arbitrarily chosen point. We characterise the distribution of ϵ by determining how the expectation value of its logarithm, $\langle \ln \epsilon \rangle$ varies as a function of $\ln M$. We show that the distribution of $\ln \epsilon$ may be mapped to determining the running maximum of a Wiener process with drift. At very large values of M there is a linear dependence: $\langle \ln \epsilon \rangle \sim -\gamma \ln M$, for some exponent γ, which depends upon the parameters of the model. We find that the value of γ is equal to zero for some regions. When γ becomes equal to zero, the voids in the distribution of trajectories are not filled when we add more trajectories, whereas the voids are filled by adding more trajectories when $\gamma > 0$. We say that the edge of the region where $\gamma = 0$ marks a phase transition, which we term the *lacunarity transition*.

Section 2 will introduce the strudel model, and describe its backward iteration as well as forward iteration. Section 3 discusses a succession of models for distribution of the void size ϵ, and section 4 discusses the lacunarity transition, where the distribution of ϵ changes abruptly in the limit as the number of trajectories M is increased. Section 5 discusses our numerical results, which show good agreement with the theory of section 3, despite the quite brutal coarse-graining approximations which are used. Section 6 contains some concluding remarks on the relation to earlier work and prospects for extension of the theory to more physically realistic models.

2. Strudel model

2.1. Definition of model

The skinny bakers' map [12] is a piecewise linear map, which mimics the stretch-and-fold action of a typical chaotic system. The unit square is stretched to twice its length in the x-direction, while being contracted by more than a factor of two in the y-direction. The stretched region is then cut into two halves which are placed in the upper and lower halves of the unit square. The unit square is, therefore, mapped into two rectangles, both of dimension $1 \times \beta/2$, where $\beta \in [0, 1]$. The resulting attractor is the Cartesian product of the unit interval and a fractal Cantor set. The fractal dimension of the attractor is $d = 1 + \ln 2/(\ln 2 - \ln \beta)$.

Our model is a variant of this skinny baker map, which we shall refer to as the *strudel model*. It is an invertible two-dimensional random dynamical system, which is designed to have regions of very low density, and to be simple enough to facilitate making analytical approximations to the distribution of sizes of empty regions. It also has the advantage that, by virtue of being a map rather than a flow, it is suited to efficient numerical work. The operation of the map is illustrated schematically by figure 2. The map depends upon two parameters, $p \in [0, 1]$ and $\beta \in [0, 1]$. It acts on a point (x, y) in the unit square, as described by equations (1) and (2)

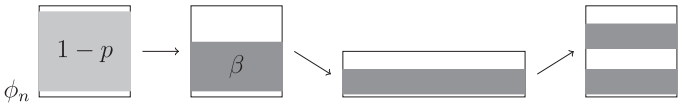

Figure 2. Illustrating the action of the strudel map. At the first step, there is a continuous, piecewise linear transformation of the y-coordinate of the unit square, which maps a region of length $1-p$ to length β. The lower edge of this region is at a random position, ϕ_n. This region is then stretched along the x-axis, to occupy a $2\times 1/2$ rectangle. This rectangle is cut and the two halves are stacked back into the unit square.

below. In the first step, a unit square is subjected to a continuous, piecewise linear, transformation of the y component. The square is then stretched by a factor of 2 in the x-coordinate, and contracted by a factor of 2 in the y-direction. The $2\times 1/2$ rectangle is then cut into two halves, which are moved back into the unit square.

To describe the transformation of the y-coordinate, we define a periodic function, $F(x) = F(x+1)$ by specifying its values on $[0,1]$ as follows:

$$F(x) = \begin{cases} \dfrac{\beta}{1-p}x & x\in[0,1-p] \\ \beta + \dfrac{1-\beta}{p}(x+p-1) & x\in[1-p,1] \end{cases}. \tag{1}$$

Also let n be the index of the iteration and let ϕ_n be a random number, with a probability density which is uniform on $[0,1]$ (and zero elsewhere), chosen independently at each iteration. Then we define the *strudel map* as follows:

$$\begin{aligned} x_{n+1} &= 2x_n \bmod 1 \\ y_{n+1} &= \frac{1}{2}[F(y_n-\phi_n) + \mathrm{int}(2x_n)], \end{aligned} \tag{2}$$

where $\mathrm{int}(x)$ is the largest integer less than x. If we set $\phi_n = 0$ and $p = 0$, this is the skinny baker map [12], which has empty regions which occupy a fraction $1-\beta^N$ of the phase space after N iterations. When $p > 0$, there are no inaccessible regions because $F(x)$ has an inverse function on $[0,1]$, but as $p\to 0$ the density of some regions may be very small.

One motivation for introducing the random phase ϕ_n is to eliminate correlations between different applications of the map. The derivatives of the map of the y-coordinate are either $(1-\beta)/2p$ or $\beta/2(1-p)$. Because of the random shift ϕ_n, these are applied independently at each application of the map. We can then give expressions for the Lyapunov exponents of this model. Small separations in the x-coordinate are doubled upon each iteration. If we also define

$$\xi_1 = \ln\left(\frac{1-\beta}{2p}\right), \quad \xi_2 = \ln\left(\frac{\beta}{2(1-p)}\right) \tag{3}$$

then the logarithm of the small separation in the y-coordinate is incremented by either ξ_1 or ξ_2 with probability p or $1-p$ respectively. The Lyapunov exponents are therefore

$$\lambda_1 = \ln 2, \qquad \lambda_2 = p\xi_1 + (1-p)\xi_2. \tag{4}$$

We note that if the random ϕ_n were *not* included, the derivatives at successive steps would be correlated, and it would be impossible to derive the above simple expressions for the Lyapunov exponents.

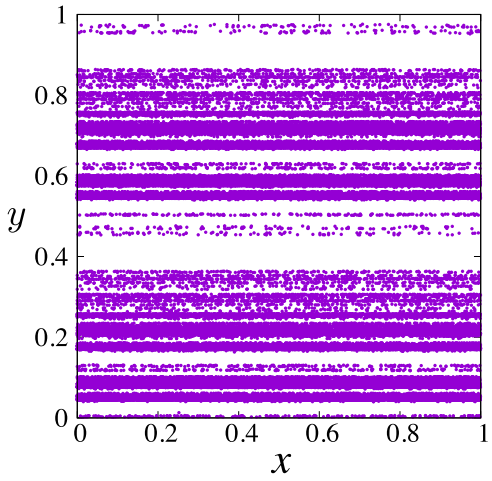

Figure 3. Distribution of trajectories for a realisation of the strudel map. The parameter values are $p = 0.2$, $\beta = 0.4$. We mapped $M = 10^5$ randomly scattered initial conditions for $N = 15$ iterations. Note that these are some substantial gaps in the distribution of the y-coordinate. These correspond to rectangular voids, of dimension $1 \times \epsilon$. We shall characterise these voids by calculating $\langle \ln \epsilon \rangle$.

We emphasise that the voids will be determined by computing $N \gg 1$ iterations of the map with $M \gg 1$ randomly scattered initial conditions, using a particular choice of the sequence $\{\phi_n, n = 1 \ldots N\}$. After N iterations the sizes of the void regions are determined. This process is then repeated for a different randomly chosen sequence of the phases, ϕ_n. The objective is to understand the statistics of the void regions, averaged over different realisations of the ϕ_n. For a given realisation of the ϕ_n, the distribution of the phase points after N iterations is highly inhomogeneous. However, the averages over distributions of the ϕ_n must be homogeneous in phase space.

For completeness, we also mention Renyi dimensions. Two of these are easily determined. If $p > 0$, the box counting dimension is $d_0 = 2$ after any finite number of iterations, because there are no inaccessible points (and hence no empty boxes). The information dimension as estimated by the Kaplan–Yorke formula [13] is

$$d_1 = 1 + \frac{\lambda_1}{|\lambda_2|} = 1 + \frac{\ln 2}{\left| p \ln\left(\frac{1-\beta}{2p}\right) + (1-p)\ln\left(\frac{\beta}{2(1-p)}\right)\right|} \tag{5}$$

(provided that $\lambda_2 < 0$, which is always true, as shown in appendix B). The distribution of points generated by this map is a random scatter in the x-direction, but highly inhomogeneous in the y-coordinate. An example is shown in figure 3. The striated texture of this image resembles the fine structure of the foliations shown in figure 1.

2.2. Pre-images

Consider the distribution obtained from $M \gg 1$ points, which are initially uniformly scattered on the unit square, after $N \gg 1$ iterations. Because the iteration of x is a Bernouilli map, which has a constant function as its invariant density, these points end up uniformly scattered in the x-coordinate. The distribution of values of the y-coordinate, however, becomes highly inhomogeneous, as illustrated in figure 3. Let us sort the y-coordinates of the points representing

trajectories into ascending order. If we then pick a point at random, it can be placed inside a rectangular void, of dimensions $1 \times \epsilon$, with trajectories on the upper and lower edges. The values of the gap size ϵ in the y-coordinate are random variables. We can characterise the lacunarity of the distribution of trajectories by determining the PDF of ϵ, or by determining its statistics.

Considering the forward propagation of a randomly chosen phase point would be a difficult approach to characterising voids. This is because sparse regions arise from the expansion of small areas, which could represent a very small fraction of the phase space. In order to understand the origin of sparse regions at a particular point in time it is much easier to follow a trajectory backwards in time from a randomly chosen point. The linearised map in the vicinity of this trajectory should be calculated. Those points which have a contracting neighbourhood in the backward-propagated map correspond to sparse regions.

To understand the statistics of these void regions, notice that all of the pre-images of a void are also empty regions (because if the pre-image were to contain a point, this point would not be mapped into the void region). If we follow the evolution backwards by N steps to the initial configuration, all of the pre-images are also empty. After n steps backwards, the area of the pre-image of the $1 \times \epsilon$ rectangle is denoted by A_n, and the area of the initial empty region is A_N. Because the initial distribution is a random scatter of M points in the unit square, the probability of an area A in the initial configuration being empty is $P(A) = \exp(-MA)$, so that the probability of the area of the N step pre-image being a large multiple of $1/M$ is very small. This implies that, (apart from rare exceptional cases), the large gaps in the y-coordinate arise as a consequence of having small areas of the pre-image.

Let us consider the sequence of pre-images of a rectangular region of size $1 \times \epsilon$ which has its lower edge at y, after N steps backwards. To facilitate the discussion, we proceed by a sequence of stages: first we obtain an expression for the pre-image of a point, then use this to understand the pre-images of horizontal and vertical line segments, which can be combined to understand the pre-image of a rectangle.

The forward map is defined by equation (2), with $F(x)$ defined by (1). We define a function G that is the inverse of F:

$$G(F(x)) = x \tag{6}$$

that is

$$G(x) = \begin{cases} \dfrac{1-p}{\beta}x & x \in [0, \beta] \\ 1 - p + \dfrac{p}{1-\beta}(x-\beta) & x \in [\beta, 1] \end{cases}. \tag{7}$$

We extend the definition of $G(x)$ to the whole real line as a periodic function with unit period. Noting that equation (2) implies that $\mathrm{int}(2x_n) = \mathrm{int}(2y_{n+1})$, we have $2y_{n+1} - \mathrm{int}(2y_{n+1}) = F(y_n - \phi_n)$, so acting on this relation with G we obtain

$$y_n = \phi_n + G(2y_{n+1}) - \mathrm{int}(2y_{n+1}), \tag{8}$$

where we use the fact that $G(\mathrm{int}(2y_{n+1})) = \mathrm{int}(2y_{n+1})$, because, by inspection of (7), if $z \in [0, 1)$, then $G(\mathrm{int}(z)) = G(0) = 0$, and if $z \in [1, 2)$ then $G(\mathrm{int}(z)) = G(1) = 1$. Equation (8) has the nice feature that it is independent of the x_n coordinate. Also, because the function G has been constructed to be periodic with unit period, we can simplify further by applying the following backward iteration:

$$\tilde{y}_n = \phi_n + G(2\tilde{y}_{n+1}) \tag{9}$$

and recover the value of y_n by subtracting the integer part. (This follows from noting that, because $G(x+1) = G(x)$, the values of y_n and $\tilde{y}_n$ always differ by an integer. Because $y_n \in [0,1]$, the value of y_n can be obtained from $\tilde{y}_n$ by subtraction of its integer part.) The forward iteration of the x-coordinate is a Bernouilli map, for which every point has two pre-images which differ by $1/2$, but in (2) the value of y_{n+1} depends upon $\mathrm{int}(2x_n)$, so that the pre-image of x_{n+1} for the map is in fact well-defined.

Next consider the pre-images of horizontal and vertical line segments. From the x-component of (2), the pre-image of a horizontal line segment of length Δx is an interval of length $\Delta x/2$. The pre-image of any vertical line which crosses the horizontal line $y = 1/2$ consists of two vertical line segments, with horizontal separation equal to one half, and with the y coordinates equal at the point of discontinuity. Finally, building a rectangle of dimensions $\Delta x \times \Delta y$ as a Cartesian product of two line segments, the pre-images of this rectangle are either one or various rectangles. Their width is $\Delta x/2$, and the total height of the pre-image rectangles is determined by applying (8) to the upper and lower edges.

Consider the backward iteration of an $1 \times \epsilon$ rectangular region, where the lower and upper edges are two successive values of the y-coordinate after N iterations, differing by ϵ, with the lower edge at y_n. After N backward steps, this maps to a set of rectangular regions, each one of which has width $\Delta x = 2^{-N}$. The sum of the vertical extent of each fragment is $\Delta\tilde{y}$, which is iterated according to

$$\Delta\tilde{y}_n = G(2y_{n+1} + 2\Delta\tilde{y}_{n+1}) - G(2y_{n+1}) \tag{10}$$

(obtained from taking the difference of between two instances of equation (9), starting with $\Delta\tilde{y}_N = \epsilon$. The pre-image of the $1 \times \epsilon$ rectangle is a set of rectangular regions of total area

$$A_N = 2^{-N}\Delta\tilde{y}_N. \tag{11}$$

If $\epsilon \ll 1$, the iteration of (10) can be approximated by linearisation, using $G(2y + 2\Delta\tilde{y}) - G(2y) = 2G^{'}(y)\Delta\tilde{y} + O(\Delta\tilde{y}^2)$), so that after N steps of backward iteration the total vertical extent of the pre-image area is

$$\Delta\tilde{y}_N \sim 2^N \epsilon \prod_{i=1}^{N} G'(2y_n). \tag{12}$$

Thus $\Delta\tilde{y}_n$ typically grow under iteration, and the approximation (12) ceases to be valid when $\Delta\tilde{y}$ is of order one.

We note that the Lyapunov exponents for the backward propagation are different from the forward Lyapunov exponents. Defining $\bar{\xi} = \ln 2G'$, we see that $\bar{\xi}$ takes two possible values, which occur randomly and independently in the sequence of y_n values:

$$\begin{aligned} \bar{\xi}_1 &= \ln\left(\frac{2(1-p)}{\beta}\right) \quad \text{probability } p_1 = \beta \\ \bar{\xi}_2 &= \ln\left(\frac{2p}{1-\beta}\right) \quad \text{probability } p_2 = 1-\beta. \end{aligned} \tag{13}$$

The Lyapunov exponents of the backward iterated map are then

$$\bar{\lambda}_1 = \beta\bar{\xi}_1 + (1-\beta)\bar{\xi}_2, \qquad \bar{\lambda}_2 = -\ln 2. \tag{14}$$

3. Model for distribution of void sizes

3.1. Representation in logarithmic variables

Consider the pre-image of a rectangular region of size $1 \times \epsilon$ after n backwards iterations. It is mapped to a set of rectangular regions of total area $A_n = \Delta x \times \Delta\tilde{y}$. While $\Delta\tilde{y}_n \ll 1$ its evolution is well approximated by

$$A_n \sim \epsilon \prod_{j=1}^{n} G'(2y_j), \tag{15}$$

where $G'(2y_j)$ takes one of two values, $(1-p)/\beta$ or $p/(1-\beta)$, with probabilities $p_1 = \beta$ or $p_2 = 1-\beta$, respectively. After $\Delta\tilde{y}$ has grown to be of order unity, the area $A_n = \Delta x_n \Delta\tilde{y}_n$ of the pre-image set stabilises, at a value denoted by $\tilde{A}$. The size of the open interval, ϵ, is determined by the condition that $\Delta\tilde{y}_n$ never exceeds unity, while the area of the pre-image reduces to $1/M$ or less.

It is convenient to use logarithmic variables:

$$X_1 = \ln \Delta x, \qquad X_2 = \ln \Delta\tilde{y}. \tag{16}$$

The backwards evolution of X_1 is trivial, and the evolution of X_2 follows from equation (12): after N backwards steps we have

$$X_1 = -N \ln 2, \qquad X_2 = \ln \epsilon + N \sum_{j=1}^{N} \bar{\xi}_j, \tag{17}$$

where the $\bar{\xi}_j$ take one of two values as specified by equation (13).

Note that the condition $\Delta\tilde{y} \leqslant 1$ corresponds to the constraint $X_2 \leqslant 0$. In terms of the logarithmic variables, the condition that $\tilde{A} \leqslant 1/M$ is

$$X_1 + X_2 \leqslant -\ln M, \tag{18}$$

and the dynamical process describing the evolution of the pre-image is therefore a random walk in X_2, as a function of X_1. The initial condition is $(X_1, X_2) = (0, \ln \epsilon)$. The point moves to the left in (X_1, X_2) space by $\ln 2$ at each step. The motion proceeds until (18) is satisfied, and we choose the largest value of ϵ so that X_2 never exceeds zero. When $\Delta\tilde{y} = 1$, the area is $A_N = \Delta x \Delta\tilde{y} = 2^{-N}$, so that the number of backward iterations is

$$N = \frac{\ln M}{\ln 2} \tag{19}$$

(which achieves $\tilde{A} = 1/M$) or greater (which results in a smaller pre-image). The trajectory in (X_1, X_2) space is illustrated in figure 4.

3.2. Modelling by Wiener process

Next we make a further simplifying assumption, which enables us to approximate the statistics of the void sizes by simple analytic formulae. The motion of X_2 as a function of X_1 defined by equation (17) is a biased random walk. It can be modelled as a Wiener process, $x(t)$ where $t \equiv -X_1$ and $x \equiv X_2$. This Wiener process has a drift velocity v and a diffusion coefficient D.

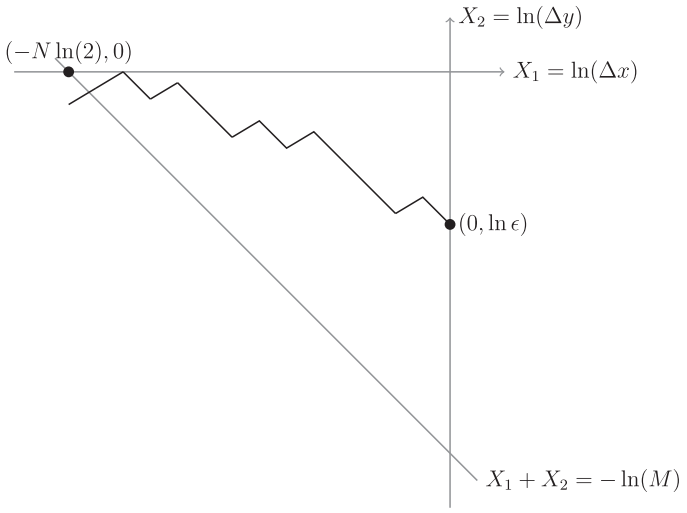

Figure 4. Schematic illustration of the dynamics determining void size, expressed in logarithmic coordinates, equation (16), as represented by equation (17). The trajectory starts from $(0, \ln\epsilon)$ and makes a biased random walk, until it exits the triangular region $X_1 + X_2 < -\ln M$. The value of ϵ is chosen so that the trajectory never enters the region $X_2 > 0$.

The mean and variance of the change in x over one timestep, $\Delta t = \ln 2$, are $v\Delta t = p_1\bar{\xi}_1 + p_2\bar{\xi}_2$, and $2D\Delta t = p_1\bar{\xi}_1^2 + p_2\bar{\xi}_2^2 - v^2\Delta t^2$, so that

$$v = \frac{p_1\bar{\xi}_1 + p_2\bar{\xi}_2}{\ln 2} = \frac{\bar{\lambda}_1}{\ln 2} \tag{20}$$

and

$$D = \frac{1}{2\ln 2}\left[p_1\bar{\xi}_1^2 + p_2\bar{\xi}_2^2 - (p_1\bar{\xi}_1 + p_2\bar{\xi}_2)^2\right]. \tag{21}$$

For each realisation of the Wiener process, we must determine the largest value of $x_0 = \ln\epsilon < 0$ such that if $x(t)$ starts at x_0, it remains negative for all times t up to

$$T = N\ln 2 = \ln M. \tag{22}$$

Alternatively, we can shift the initial condition and consider a Wiener process which starts at $x(0) = 0$, and then $-\ln\epsilon$ is the maximum value of a Wiener process $x(t)$ in the time interval $t \in [0, T]$. This alternative approach is illustrated schematically in figure 5.

3.3. Estimate for mean value

Now let us estimate the mean value of $x_0 = \ln\epsilon$, using the Wiener process model. If the diffusion coefficient were $D = 0$, and $v > 0$, and we were to release a particle at $x_0 = -vT$, then it would reach $x = 0$ when $t = T$. In this deterministic case we would have $\langle x_0\rangle = -vT$. On the other hand, if $v = 0$ we would expect that the maximum displacement would be of order $\sqrt{DT}$. If diffusion is significant, but $v \neq 0$, we might, therefore, anticipate that

$$\langle x_0\rangle = -\sqrt{2DT}F(Y), \tag{23}$$

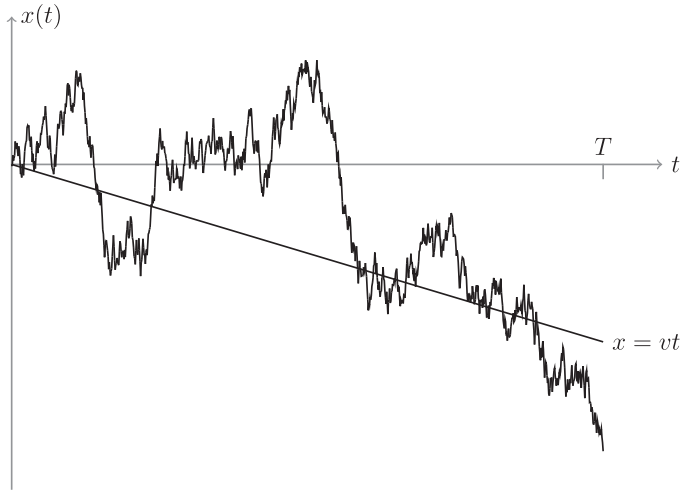

Figure 5. Schematic illustration of the dynamics determining void size, expressed in logarithmic coordinates, where the biased random walk is approximated by a Wiener process. We require the statistics of the running maximum of the Wiener process $x(t)$, up to time T, which is equal to $-\ln\epsilon$.

where $F(Y)$ is a function of a dimensionless variable

$$Y = v\sqrt{\frac{T}{2D}} \tag{24}$$

and where $F(Y) \sim Y$ as $Y \to \infty$. In the appendix C we show that the function $F(Y)$ is

$$F(Y) = \Phi'(Y) + \Phi(Y)\frac{1+Y^2}{Y} - \frac{1}{2Y}, \tag{25}$$

where

$$\Phi(x) = \frac{1}{\sqrt{2\pi}}\int_{-\infty}^{x} \mathrm{d}y\ \exp(-y^2/2) \tag{26}$$

is the cumulative distribution function of a Gaussian with unit variance. The limiting behaviours of $F(Y)$ are

$$F(Y) \sim \begin{cases} Y & Y \gg 1 \\ \sqrt{\dfrac{2}{\pi}} & Y = 0 \\ \dfrac{1}{2|Y|} & -Y \gg 1 \end{cases}. \tag{27}$$

4. Lacunarity transition

We have proposed a theory for the statistic $\langle \ln\epsilon \rangle$, where ϵ characterises the size of a void region. In the limit as the number of trajectories M approaches infinity, the dimensionless variable Y

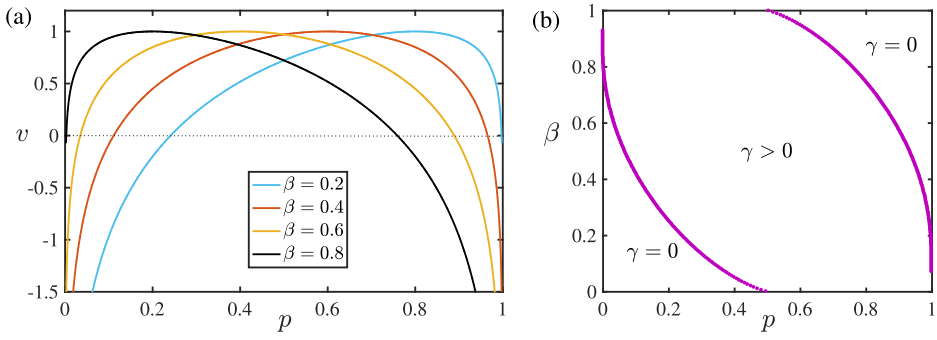

Figure 6. (a) Plots of v as a function of p for $\beta = 0.2, 0.4, 0.6, 0.8$. The dotted line indicates $v = 0$ for reference. (b) Plot of the (p, β) parameter space of the model. The purple lines correspond to the locus of the phase transition, with $\gamma > 0$ in the region between the lines and $\gamma = 0$ everywhere else.

defined by (24) is large, and according to equations (23) and (27) the theory predicts that

$$\langle \ln \epsilon \rangle \sim -v \ln M, \tag{28}$$

where v is given by equation (20), provided that $v > 0$. This is consistent with the typical size of ϵ having a power-law dependence:

$$\epsilon \sim M^{-\gamma}, \tag{29}$$

where the exponent is $\gamma = v$. If $\gamma < 1$ this indicates that the voids are larger than would be expected for a random scatter of points, for which the separation of the ordered y-coordinates would be $\epsilon \sim 1/M$.

In the case where $v < 0$, however, $Y \to -\infty$ as $M \to \infty$, and the theory predicts that $\langle \ln \epsilon \rangle$ becomes independent of M as $M \to \infty$, so that $\gamma = 0$ in regions where $v < 0$. Numerical investigations of equation (20), illustrated in figure 6 below, indicate that there is indeed a region in the parameter space of our model where $v < 0$. In this case $\langle \ln \epsilon \rangle \sim D/v$, which is independent of M. This implies that when $v < 0$, there are voids in the distribution of trajectories which are not filled as we increase their number. The locus where $v = 0$ in the parameter space of the model $\{p, \beta\} \in [0, 1]^2$ represents a phase transition, between a phase space which fills every region as $M \to \infty$ when $v > 0$, to one which has persistent voids when $v < 0$.

The value of v as a function of p for different choices of β is shown in figure 6(a). The line of the phase transition in the (p, β) parameter space is illustrated in figure 6(b).

The condition for the phase transition to occur has a very simple interpretation. If both of the Lyapunov exponents of the time-reversed flow are negative, then the neighbourhood of any point almost certainly contracts as we go backwards in time. This means that almost all points are surrounded by a neighbourhood which is increasingly sparse. Because $\bar{\lambda}_2$ is always negative, the phase transition occurs when $\bar{\lambda}_1 = 0$, or equivalently when $v = 0$.

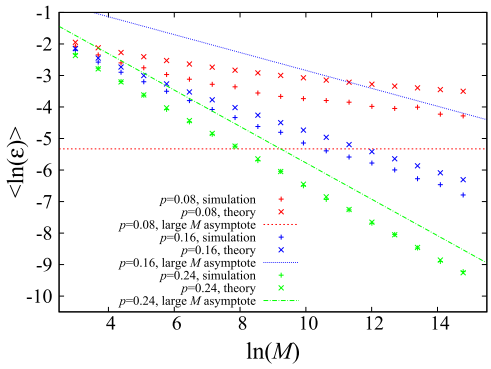

Figure 7. Plots of $-\langle \ln \epsilon \rangle$ as a function of $T = \ln M$, for $\beta = 0.4$, with three different values of p. These data are compared with the theory, equations (23) and (25): the fractional error of the theory decreases as $|\langle \ln \epsilon \rangle|$ increases. The dotted lines are the asymptotes of the theory for very large values of M, showing that even 10^6 trajectories are not sufficient to explore the $M \to \infty$ limit.

5. Numerical simulations

We evaluated the values of $-\langle \ln \epsilon \rangle$, after $N = 100$ iterations of the map. We averaged $N_r = 500$ realisations of the map, and in each case we evaluated the set of void sizes ϵ using $K = 250$ evenly spaced initial points. The resulting expectation values of $\ln \epsilon$ are compared with the theoretical prediction, equations (23) and (25) in figure 7 for three different points in the parameter space of the model. The agreement between the simulations and equation (23) is excellent in one case ($\beta = 0.4$ and $p = 0.24$), but the other two cases show a small offset between the simulation and this theoretical prediction, which is approximately independent of M.

Replacing a discrete random walk by a Wiener process is a 'coarse-grained' approximation of the random walk, which is expected to work well in the long-time limit (equivalently, in the limit where the number of trajectories is very large). The data in figure 7 indicate that the fractional error of the approximation is decreasing as $T = \ln M$ increases, while $|\langle \ln \epsilon \rangle|$ increases.

The values of the drift velocity and diffusion coefficient for the three cases illustrated in figure 7 are:

$$\begin{aligned} &\text{for } p = 0.08,\ \beta = 0.4 \quad \to \qquad v = -0.2634\ldots,\ D = 1.4040\ldots \\ &\text{for } p = 0.16,\ \beta = 0.4 \quad \to \qquad v = 0.2840\ldots,\quad D = 0.7373\ldots \\ &\text{for } p = 0.24,\ \beta = 0.4 \quad \to \qquad v = 0.5772\ldots,\quad D = 0.4203\ldots \end{aligned} \tag{30}$$

When $v > 0$, the asymptotic behaviour as $M \to \infty$ is $\langle \ln \epsilon \rangle \sim -v \ln M$, whereas if $v < 0$, $\langle \ln \epsilon \rangle \sim D/v$. The data points in figure 7 all appear to be well approximated by a straight line when M is large. However, this figure also shows the $M \to \infty$ asymptotic behaviour as lines, and even for the largest values of M (up to $10 \times 2^{18} > 10^6$), the theoretical expression is still far from these asymptotes. We conclude that the true asymptotic behaviour is not accessible even for the very large values of M which are explored in figure 7.

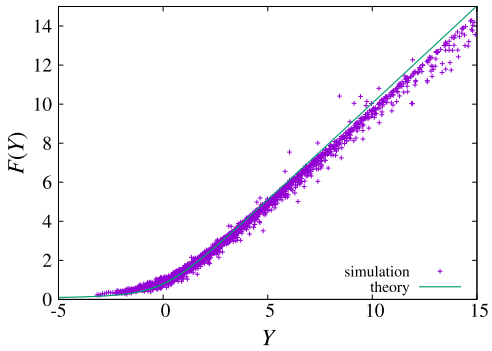

Figure 8. We evaluated the void sizes, ϵ, after $N = 100$ iterations, and determined $\langle \ln \epsilon \rangle$. This was repeated for $M = 4, 8, \ldots, 2^{19}$ trajectories, and for values of p and β on a lattice filling the parameter space. The graph shows a scatterplot of $Z = -\langle \ln \epsilon \rangle / \sqrt{2DT}$ as a function of $Y = v\sqrt{T/2D}$, for more than 10^3 different combinations of values of p, β and $T = \ln M$. These data are compared with the function $F(Y)$ (solid line), defined by equation (25).

We also evaluated $\langle \ln \epsilon \rangle$ for 18 different values of M, namely $M = 4, 8, \ldots, 2^{19}$, for all values of p and β forming a lattice in the parameter space. (The lattice spacing was 0.075, with p taking values from 0.075 to 0.9 and β from 0.15 to 0.9, making 132 different points in the parameter space). For each of these 132×18 data points we determined v and D from the values of p and β and $T = \ln M$. We then computed $Y = v\sqrt{T/2D}$ and $Z = -\langle \ln \epsilon \rangle / \sqrt{2DT}$. Figure 8 is a scatterplot of Z against Y, compared with the function $F(Y)$, given by equation (25). There is a good scaling collapse of the scatterplot onto a single line, and this line is in good agreement with the function $F(Y)$.

6. Concluding remarks

Data from both physical and numerical experiments on non-autonomous chaotic systems indicate that there can be very sparsely occupied regions of phase space. These have previously been investigated for the case of systems which have folds or caustics [11], but in the case of systems with invertible dynamics there is very little previous work.

In this paper we considered a simple model, which is susceptible to analysis by mapping the problem to that of determining the running maximum of a biased diffusion process. The model system which we consider has uniform distribution of trajectories in its x-coordinate, but a highly non-uniform distribution of the y-coordinate, as illustrated in figure 3. We considered M trajectories with uniformly scattered initial points, after N iterations of the map. A randomly chosen point (x, y) can be positioned in a rectangle of dimensions $1 \times \epsilon$, which contains none of the trajectories in its interior, but which does have one trajectory on its upper and lower edges. The statistics of the gap size, ϵ, provide a means to describe figure 3. We developed a theory for $\langle \ln \epsilon \rangle$, predicting that $\langle \ln \epsilon \rangle \sim -\gamma \ln M$ as $\ln M \to \infty$, where γ is a positive coefficient which depends upon the parameters of the model. This relationship is consistent with ϵ having a power-law relation to the number of trajectories, $\epsilon \sim M^{-\gamma}$, but (as illustrated by figure 7) the approach to this limiting power-law can be so slow that the exponent cannot be seen in numerical simulations.

As well as having a power-law dependence, $\epsilon \sim M^{-\gamma}$, in the limit as $M \to \infty$, there is a transient behaviour at finite values of M. We showed that this transient behaviour can be described quite accurately by a 'coarse-grained' approximation of the equations describing our model, replacing a random walk with a Wiener process.

We argued that varying parameters of this model system can cause a transition, from a phase in which γ is positive, to regions of parameter space in which it is zero. It is, however, difficult to observe a sharp phase transition upon varying parameters of the model, because the width of the transition region, where the limiting slope of the plot of $\langle \ln \epsilon \rangle$ versus $\ln M$ becomes established, increases as $\gamma \to 0$. Equations (23) and (24) imply that the width of this transition region is $\ln M^* \sim D/v^2$, so that seeing the change of slope in the transition region required a very large number of trajectories, $M^* \sim \exp(2D/v^2)$.

In the introduction we mentioned that the concept of multifractal measures appears as if it may be relevant to our investigation. The power-law relation $\epsilon \sim M^{-\gamma}$ is consistent with the 'multifractal' model, in that it represents an exponent which characterises the dimension of the measure in the vicinity of a point. However, the exponent γ is the same for almost all points in the phase space, rather than different values of γ being realised on sets which have a fractal structure. Also, as illustrated in figure 7, the convergence towards a power-law as the number of trajectories increases can be so slow that it is not observable.

Figure 1 showed voids in the distribution of a physically interesting invertible, non-autonomous chaotic system. It is interesting to consider how the approach used on our simplified model can be extended to understand the distribution of the distance ε from a randomly chosen point to the nearest one of M trajectories in more general cases. As in the case of the simplified model that we have considered here, the simplest way to understand the statistics of ε is to propagate the dynamics backwards in time. All of the pre-images of this ε ball are also empty. In particular, the pre-image at time zero does not contain any of the initial random distribution of trajectories. Because the trajectories were assumed to be randomly scattered at time zero, the pre-image set at $t = 0$ is very unlikely to have an area which exceeds $1/M$ by a large factor.

Consider the form of the pre-images of a small ball of radius ε. The evolution of this set under backward time evolution is, at least initially, described by the linearisation of the flow. In many examples, including the case illustrated in figure 1, the pre-image of a ball is initially transformed into an ellipse with one principal axis increasing and the other one decreasing, such that the area is contracting. Eventually, the linearisation approximation fails, when the size of the larger principal axis of the ellipse approaches unity. Upon further backward propagation, the pre-image set is a string-like object, which eventually becomes foliated so that it covers the whole of the phase space with uniform density. When this happens, the area remains approximately constant as we propagate backwards in time, because the dynamics preserves the total area. This picture is quite analogous to our treatment of the strudel model, but the machinery of the calculations will be more complex. We expect to explore the generalisation to more complex dynamical systems in a subsequent paper.

Acknowledgments

MW acknowledges hospitality of the Chan-Zuckerberg Biohub, and discussions with John Hannay about different approaches to the derivation of equation (25). MP acknowledges financial support by the UK Engineering and Physical Sciences Research Council (EPSRC) through Grant No. EP/R041954/1.

Data availability statement

The data that support the findings of this study are available upon reasonable request from the authors.

Appendix A. Advective flow model

The trajectories shown in figure 1 are generated by numerically solving the two-dimensional flow

$$\boldsymbol{x}(t+\Delta t) = \boldsymbol{x}(t) + \boldsymbol{u}(\boldsymbol{x}, t)\Delta t, \tag{31}$$

with the random velocity field $\boldsymbol{u}(\boldsymbol{x}, t)$ defined as

$$\boldsymbol{u} = \nabla \wedge \boldsymbol{\psi} + \beta \nabla \phi, \tag{32}$$

where β is a compressibility parameter, $\boldsymbol{\psi}(x, y)$ is a random stream function and $\phi(x, y)$ is a random potential. In the simulations of figure 1 we used $\beta = 0.5$ and the fields $\boldsymbol{\psi}(x, y)$ and $\phi(x, y)$ were chosen to be independent, have zero mean values, and have the same Gaussian correlation function, with rotationally and translationally invariant statistics.

Appendix B. Proof λ_2 is negative

The Lyapunov exponent $\lambda_2(\beta, p)$ is

$$\lambda_2 = p \ln\left(\frac{1-\beta}{2p}\right) + (1-p)\ln\left(\frac{\beta}{2(1-p)}\right) \tag{33}$$

for $\beta \in [0, 1]$ and $p \in [0, 1]$. To show that λ_2 is always negative we will show that its maximum is $-\ln 2$ (independent of the value of p). We find that $\partial\lambda_2/\partial\beta = 0$ is satisfied when $\beta + p = 1$, and that $\lambda_2(1-p, p) = -\ln 2$. Furthermore,

$$\frac{\partial^2\lambda_2}{\partial\beta^2} = -\left(\frac{p}{(1-\beta^2)^2} + \frac{1-p}{\beta^2}\right) < 0, \tag{34}$$

which is negative for all values of p and β, and so $\lambda_2(\beta)$ is a concave function, which takes its maximum at $\beta = 1 - p$.

Appendix C. Derivation of expectation value of maximum of Wiener process

In [14] there is an analysis of the solution of the advection diffusion equation, with drift velocity v and diffusion coefficient D. It is shown that the flux onto an absorbing point at $\bar{x}$ from a source at $x = 0$, $t = 0$ is

$$J(\bar{x}, t) = \frac{\bar{x}}{\sqrt{4\pi D t^3}} \exp\left[-\frac{(\bar{x} - vt)^2}{4Dt}\right]. \tag{35}$$

The probability that a particle has a maximum excursion which is less that $\bar{x}$ before time t is equal to the probability that it is not absorbed onto that surface, namely

$$P(\bar{x},t) = 1 - \int_0^t \mathrm{d}t'\, J(\bar{x},t'). \tag{36}$$

The corresponding probability density for $\bar{x}$ is $p(\bar{x},t) = \partial P/\partial \bar{x}$, so that the expectation value of $\bar{x}$ is

$$\langle \bar{x} \rangle = -\int_0^t \mathrm{d}t' \int_0^\infty \mathrm{d}\bar{x}\, \bar{x} \frac{\partial J}{\partial \bar{x}}(\bar{x},t') = \int_0^t \mathrm{d}t' \int_0^\infty \mathrm{d}\bar{x}\, J(\bar{x},t'). \tag{37}$$

That is, defining $Z = v\sqrt{t'/2D}$ and $Y = v\sqrt{t/2D}$,

$$\begin{aligned}
\langle \bar{x} \rangle &= \frac{1}{\sqrt{4\pi D}} \int_0^t \mathrm{d}t'\, \frac{1}{t'^{3/2}} \int_0^\infty \mathrm{d}\bar{x}\, \bar{x} \exp\left[-\frac{(\bar{x} - vt')^2}{4Dt'} \right] \\
&= \frac{1}{\sqrt{2\pi}} \int_0^t \mathrm{d}t'\, \frac{1}{t'} \int_{-v\sqrt{t'/2D}}^\infty \mathrm{d}\omega \left[\sqrt{2Dt'}\omega + vt' \right] \exp\left(-\frac{\omega^2}{2} \right) \\
&= \sqrt{\frac{D}{\pi}} \int_0^t \frac{\mathrm{d}t'}{\sqrt{t'}} \int_{-Z}^\infty \mathrm{d}\omega\, \omega \exp\left(-\frac{\omega^2}{2} \right) \\
&\quad + \frac{v}{\sqrt{2\pi}} \int_0^t \mathrm{d}t' \int_{-Z}^\infty \mathrm{d}\omega \exp\left(-\frac{\omega^2}{2} \right) \\
&= \sqrt{\frac{D}{\pi}} \int_0^t \frac{\mathrm{d}t'}{\sqrt{t'}} \exp\left(-\frac{Z^2}{2} \right) + v \int_0^t \mathrm{d}t'\, \Phi(Z) \\
&= \frac{4D}{v} \frac{1}{\sqrt{2\pi}} \int_0^Y \mathrm{d}Z \exp\left(-\frac{Z^2}{2} \right) + \frac{4D}{v} \int_0^Y \mathrm{d}Z\, Z\, \Phi(Z) \\
&= \frac{2}{Y}\sqrt{2Dt} \left[\Phi(Y) - \frac{1}{2} + \frac{Y^2}{2}\Phi(Y) - \frac{1}{2\sqrt{2\pi}} \int_0^Y \mathrm{d}Z\, Z^2 \exp\left(-\frac{Z^2}{2} \right) \right] \\
&= \sqrt{2Dt} \left[\frac{2}{Y}\Phi(Y) - \frac{1}{Y} + Y\Phi(Y) - \frac{1}{Y\sqrt{2\pi}} \right. \\
&\quad \left. \times \left(-Y \exp\left(-\frac{Y^2}{2} \right) + \sqrt{\frac{\pi}{2}} (2\Phi(Y) - 1) \right) \right] \\
&= \sqrt{2Dt} \left[\Phi(Y) \left(Y + \frac{1}{Y} \right) + \Phi'(Y) - \frac{1}{2Y} \right] \\
&= \sqrt{2Dt}\, F(Y),
\end{aligned} \tag{38}$$

where $F(Y)$ is the function specified in equation (25). There are other sources which could be used to obtain (23) and (25), for example a book by Borodin and Salminen ([15], see part II, ch 2, equation (1.1.4), p 250), although there is an error in the published formula.

ORCID iDs

Marc Pradas https://orcid.org/0000-0002-8814-2403
Michael Wilkinson https://orcid.org/0000-0002-5131-9295

References

[1] Sommerer J and Ott E 1993 Particles floating on a random flow: a dynamically comprehensible physical fractal *Science* **359** 334
[2] Larkin J, Bandi M M, Pumir A and Goldburg W I 2009 Power-law distributions of particle concentration in free-surface flows *Phys. Rev.* E **80** 066301
[3] Ott E 2002 *Chaos in Dynamical Systems* 2nd edn (Cambridge: Cambridge University Press)
[4] Bec J, Gawędzki K and Horvai P 2004 Multifractal clustering in compressible flows *Phys. Rev. Lett.* **92** 224501
[5] Wilkinson M and Grant J 2018 A matrix contraction process *J. Phys. A: Math. Theor.* **51** 105002
[6] Mandelbrot B B 1982 *The Fractal Geometry of Nature* (San Francisco: W.H. Freeman & Co Ltd)
[7] Plotnick R E, Gardner R H, Hargrove W W, Prestegaard K and Perlmutter M 1996 Lacunarity analysis: a general technique for the analysis of spatial patterns *Phys. Rev.* E **53** 5461–8
[8] Tolle C R, McJunkin T R, Rohrbaugh D T and LaViolette R A 2003 Lacunarity definition for ramified data sets based on optimal cover *Physica* D **179** 129–52
[9] Halsey T C, Jensen M H, Kadanoff L P, Procaccia I and Shraiman B I 1986 Fractal measures and their singularities: the characterization of strange sets *Phys. Rev.* A **33** 1141–51
[10] Salat H, Murcio R and Arcaute E 2017 Multifractal methodology *Physica* A **473** 467–87
[11] Wilkinson M, Pradas M, Huber G and Pumir A 2019 Lacunarity exponents *J. Phys. A: Math. Theor.* **52** 115101
[12] Alexander J C and Yorke J A 1984 Fat baker's transformations *Ergod. Theor. Dynam. Syst.* **4** 1–23
[13] Kaplan J L and Yorke J A 1979 Chaotic behaviour of multidimensional difference equations *Functional Differential Equations and Approximation of Fixed Points* (*Lecture Notes in Mathematics* vol 730) ed H-O Peitgen and H-O Walther (Berlin: Springer) pp 223–37
[14] Grant J and Wilkinson M 2015 Advection-diffusion equation with absorbing boundary *J. Stat. Phys.* **160** 622–35
[15] Borodin A N and Salminen P 2002 *Handbook of Brownian Motion: Facts and Formulae* 2nd edn (Basel: Birkhäuser)